ACS APPLIED MATERIALS & INTERFACES

Research Article

www.acsami.org

Synthesis and Growth Mechanism of Thin-Film TiO_2 Nanotube Arrays on Focused-Ion-Beam Micropatterned 3D Isolated Regions of Titanium on Silicon

Hoda Amani Hamedani,*[,†] Simon W. Lee,[†] Abdulkareem Al-Sammarraie,[‡] Zohreh R. Hesabi,[†] Asim Bhatti,[§] Faisal M. Alamgir,[†] Hamid Garmestani,[†] and Mohammad A. Khaleel[⊥]

[†]School of Materials Science and Engineering, Georgia Institute of Technology, 771 Ferst Drive NW, Atlanta, Georgia 30332-0245, United States

[‡]Department of Chemistry, College of Science, University of Baghdad, Jadiriyah-Baghdad, Iraq

[§]Centre for Intelligent Systems Research (CISR), Deakin University, Burwood, Victoria 3217, Australia

[⊥]Fundamental and Computational Sciences Directorate, Pacific Northwest National Laboratory, Richland, Washington 99354, United States

Supporting Information

ABSTRACT: In this paper, the fabrication and growth mechanism of net-shaped micropatterned self-organized thin-film TiO_2 nanotube (TFTN) arrays on a silicon substrate are reported. Electrochemical anodization is used to grow the nanotubes from thin-film titanium sputtered on a silicon substrate with an average diameter of ~30 nm and a length of ~1.5 μm using aqueous and organic-based types of electrolytes. The fabrication and growth mechanism of TFTN arrays from micropatterned three-dimensional isolated islands of sputtered titanium on a silicon substrate is demonstrated for the first time using focused-ion-beam (FIB) technique. This work demonstrates the use of the FIB technique as a simple, high-resolution, and maskless method for high-aspect-ratio etching for the creation of isolated islands and shows great promise toward the use of the proposed approach for the development of metal oxide nanostructured devices and their integration with micro- and nanosystems within silicon-based integrated-circuit devices.

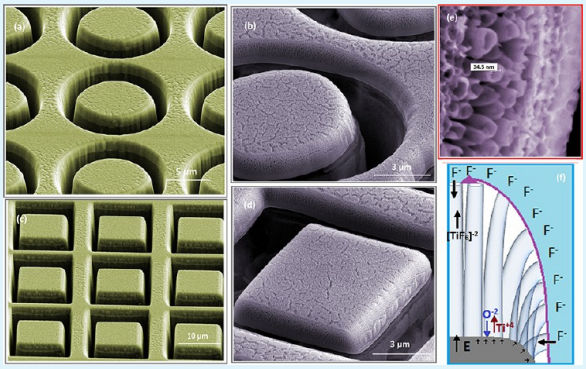

KEYWORDS: *thin-film TiO_2 nanotubes, electrochemical anodization, micropatterning, focused ion beam, XPS, XRD*

1. INTRODUCTION

As high-performance portable electronic systems are becoming vastly popular, the development of power sources and sensors together with microelectromechanical (MEM) components and other active electronics on the same silicon wafer seems to be very promising for use in portable electronic devices.[1−3] Titanium dioxide (TiO_2) is one of the most researched functional semiconductor materials and finds versatile applications in sensors, optoelectronics, dye-sensitized solar cells, photocatalysis, biomedicine, and electrochemical and storage devices such as batteries.[4−7] More recently, self-assembled one-dimensional (1D) vertically oriented TiO_2 nanotube arrays grown on different substrates have been shown to be an attractive component of such devices because of their enhanced structural properties at the nanoscale.[8−10] Of the many routes that have been used to prepare 1D arrays of metal−oxide nanotubes, including template and hydrothermal synthesis and electrochemical lithography, the electrochemical anodization process is the most promising technique with the potential for automation relative to many other methods.[11−14]

A key to the incorporation of high-surface-area, high-crystallinity TiO_2 in microelectronics applications is the directed growth of TiO_2 nanotube arrays on silicon. Such an architecture will allow the development of novel micro/nanoelectromechanical and electrochemical applications. Moreover, the high degree of biocompatibility of TiO_2-based nanostructures combined with selective growth of such organized nanoporous structures on silicon will make this material a great model system to develop nanosensors to study the response of cells. Photolithography, selective wet etching, and reactive-ion etching have been widely used for making patterned structures over large areas for various applications. Micropatterning and site-selective growth of a TiO_2 thin film, TiO_2 nanotubes on titanium foil, and thin-film TiO_2 nanotube (TFTN) arrays on a silicon wafer have been reported using versatile approaches such as on a superhydrophilic−super-

Received: June 7, 2013
Accepted: August 19, 2013
Published: August 19, 2013

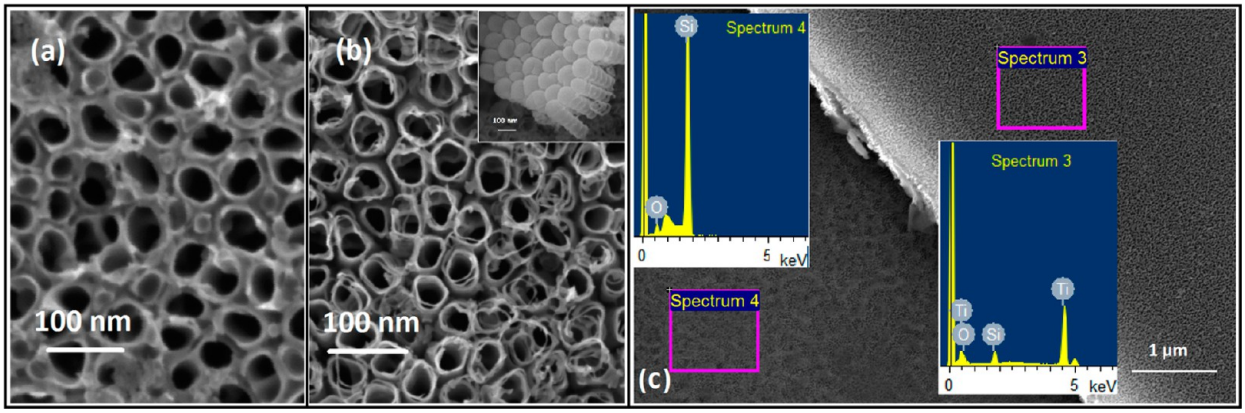

Figure 1. (a and b) Top-view FESEM images of the as-anodized and annealed TFTNs (inset: cross-sectional view of the nanotubes looking from the back side) on silicon. (c) EDS spectra showing the chemical composition of the thin film and substrate.

hydrophobic template, applying a seed layer based on the use of photolithography techniques.[15−17]

Recently, Schmuki and co-workers have reported the fabrication of photolithography micropatterned TiO_2 nanotubes, which enable highly selective bonelike hydroxyapatite formation on defined lateral microstructures of the nanotubes.[18] Despite their potential capacity for generating a large area of highly uniform periodic microarrays, photolithography-based techniques suffer from multiple complex steps. The use of polymer photoresists and the difficulty of finding suitable etching conditions particularly suited for realizing high-resolution three-dimensional (3D) patterns add drawbacks to the implementation of such methods in several practical applications.

Among all micronanopatterning techniques, focused ion beam (FIB) offers a larger variety of patterning schemes over nanolithography methods by site-specific sputtering/milling as a resistless process with the capability of direct surface modification. Moreover, compared with photolithography, the milling resolution of the ion beam makes it a suitable technique for specialty direct-write patterning with ever-higher aspect ratios.

While FIB patterning seems to be more expensive and time-consuming than standard photolithographic-based batch fabrication techniques, it offers several advantages such as improved accuracy and submicrometer feature sizes, both of which make standard photolithography challenging. In addition to that, the authors point out that FIB patterning usually does not require prepatterned masks, whose preparation time and cost significantly increase for submicrometer feature sizes.

Recently, Chen et al. have used the FIB method for the fabrication and investigation of the growth mechanism of TiO_2 nanotubes on curved surfaces and in different arrangements in a FIB-guided anodization process.[19,20] However, to the authors' knowledge, there is no report on the growth mechanism of TFTN arrays on 3D islands, where the titanium film is only connected to the substrate from underneath and is isolated from its surroundings.

In this paper, the synthesis of TFTN arrays on a silicon substrate using two different electrolyte systems is reported. The fabrication and growth mechanism of TFTN arrays on 3D isolated islands are demonstrated for the first time using the FIB technique. FIB (with a Ga^{3+} ion beam) is used for micropatterning of thin-film sputtered titanium to create isolated regions of different shapes for demonstration of the growth mechanism of TiO_2 nanotube arrays on these isolated areas with different geometries as a suggestive platform for biological cell growth studies and other types of micro-electrochemical/mechanical sensors and devices. To the authors' knowledge, this the first demonstration of the use of FIB for micropatterning of 3D isolated islands of TiO_2 nanotube arrays.

2. EXPERIMENTAL SECTION

2.1. Titanium Thin-Film Deposition. The n-type Si(100) wafers were first degreased using a standard technique followed by oxygen plasma cleaning prior to deposition. Titanium films of 800 ± 10 nm and 1.6 ± 0.01 μm thicknesses were deposited onto silicon substrates using direct-current magnetron sputtering. The chamber was first evacuated to 2.0×10^{-7} Torr backpressure, and the argon gas pressure was then maintained at 6.0×10^{-4} Torr during deposition. The sputtering power and deposition temperature were held constant at 125 W and 500 °C, respectively. The sputtering rate of titanium was found to be ∼1 Å/s, which results in deposition of a 800 ± 10-nm-thick layer of titanium in ∼135 min.

2.2. Growth of Thin-Film Titania Nanotube Arrays. Self-organized TiO_2 nanotube arrays were grown by electrochemical anodization of titanium thin films on silicon substrates in two different electrolytes. In the first route, the TiO_2 nanotube arrays were grown in a conventional two-electrode cell in an aqueous solution of 0.5 wt % HF and 1 M H_2SO_4 and at a constant temperature of 4 °C. The anodization voltage was held at a constant voltage of 10 V for 30 min and 1 h. The second route consisted of room temperature anodization of the titanium thin film in an organic electrolyte consisting of 96 wt % ethylene glycol (EG) and 0.4 g of NH_4F dissolved in 3 wt % deionized water, at a constant voltage of 40 V and for the same durations. Both TFTN array samples were annealed at 420 °C for 4 h with a heating rate of 1 °C/s to form the crystalline anatase phase.

2.3. FIB Micropatterning for 3D Isolated TiO_2 Nanotube Array Growth. The FEI Nova Nanolab 200 FIB/SEM was used for micropatterning of sputtered titanium thin films into 3D isolated cylindrical and cubic regions of titanium on a silicon substrate. The ion beam voltage and current were set to 30 kV and 5 nA, respectively. The sputter material was set to aluminum with a sputter rate value (0.3 μm^3/nC) closest to that of titanium (0.37 μm^3/nC). In order to obtain the desired mill depth, which here is the entire thickness of the titanium thin film, the Z value was calculated based on the relationship between the sputter rate, beam current, and volume of the material to be milled, as in the following equation:

$$\text{sputter rate} = \frac{\text{volume}}{\text{charge}} \tag{1}$$

where the charge is the beam current multiplied by the sputter time. FIB micropatterning of sputtered thin-film titanium was performed for

dx.doi.org/10.1021/am402203m | ACS Appl. Mater. Interfaces 2013, 5, 9026−9033

realization of high-resolution 3D (cylindrical and cubic) islands and investigation of the growth mechanism of TFTN arrays on these isolated regions on a silicon substrate using electrochemical anodization.

2.4. Characterization of Thin-Film Titania Nanotube Arrays. The morphology and composition of the TFTNs were examined using field-emission scanning electron microscopy (FESEM; Zeiss SEM Ultra60) with an energy-dispersive X-ray spectroscopy (EDS) detector. The crystal structure and thermal evolution of the TFTNs were determined by transmission electron microscopy (TEM; Jeol-2011 operated at 200 kV) and in situ high-temperature glancing-incidence X-ray diffraction (HT-GIXRD) using an X'Pert PRO MRD diffractometer with a Cu Kα radiation source. The surface properties and compositions of the samples were analyzed by X-ray photoelectron spectroscopy (XPS) using a Thermo Scientific K-Alpha system with an aluminum anode.

3. RESULTS AND DISCUSSION

3.1. Effect of an Electrolyte on the Morphology of TFTNs. The growth of the thin-film oxide nanotube layer was first monitored by studying the current−time characteristics as reported elsewhere.[21] Parts a and b of Figure 1 show the top-view FESEM images of the as-anodized and annealed TFTNs (and the cross-sectional view of the back side of the nanotubes in the inset) formed by anodization of thin-film titanium in a HF-containing aqueous electrolyte at 4 °C for 30 min and after annealing at 420 °C in air. As shown in this image, the average inner diameter and length of the as-anodized and annealed nanotubes were ∼50 and ∼300 nm, respectively; this diameter corresponds to that of the TiO_2 nanotubes grown on titanium foil and anodized at 10 V for the same duration as that reported in the literature.[9]

The formation of high-quality nanotubes in this work was shown to be only achievable below 5 °C in the HF-based aqueous electrolyte solution. This is in accordance with the findings of Macak et al., where the formation of nanotubes in a similar HF-based electrolyte has been observed at a temperature of 2 °C.[10] With monitoring of the current changes during the anodization process, the critical steps for TiO_2 formation (by oxidation of the titanium layer) and solvatization of Ti^{4+} to form the nanoporous or nanotube structure across the surface, followed by electric-field-assisted and chemical dissolution of TiO_2, were controlled. Formation of the nanotubes accompanied by the two competing electric-field-assisted and chemical dissolution processes was also found to be dependent on the anodization temperature. At temperatures higher than 5 °C, the surfaces of the nanotubes were found to be covered with some irregular features, while there was a higher chance of dissolution of the entire film. At the low-temperature range of 2−5 °C, precipitate-free nanotubes were found to be formed at a sufficiently low rate of chemical dissolution of TiO_2. Figure 1c shows the FESEM image and corresponding EDS analysis of the as-anodized TFTN layer on a silicon substrate, which confirm the chemical composition of the film as well as the substrate.

Figure 2 shows the FESEM images of smooth as-anodized and annealed TFTNs formed by anodization of thin-film titanium in a NH_4F-containing organic electrolyte at room temperature for 1 h at 40 V and after annealing at 420 °C in air. The titanium film thickness in this sample was 1.6 μm. As shown in Figure 2a, the length of the TFTNs is ∼1.3 μm, which is due to longer anodization time. Here, the sidewalls of the organic TFTNs contain some ripples formed approximately at one-third of the length from the bottom side of the nanotubes

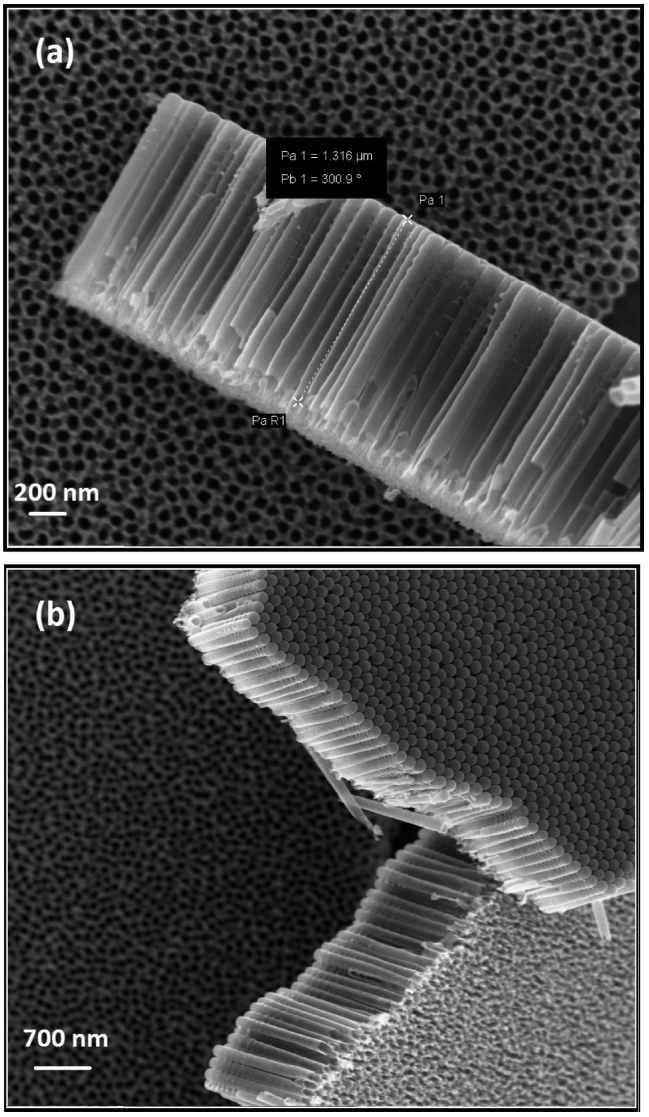

Figure 2. FESEM images of the organic TFTNs showing the top side, cross-sectional, and back side of the nanotube arrays.

due to the presence of 3% water in the electrolyte, as opposed to the aqueous TFTNs, where the entire nanotube is composed of the sidewall ripples. This effect is explained in more detail in the following section. In addition, the formation of close-packed clusters of nanotubes is observed in an EG electrolyte, where the intertubular spacings are negligible. Deviation from such a close-packed architecture and clustering of the nanotubes are reported by Mohammadpour et al.[22] In their study, the formation mechanism of very large-diameter nanotubes discretized with large intertubular spacings is discussed through a combination process of the nanotubes and their deflection mechanism to form multipodal nanotubes in a highly viscous diethylene glycol electrolyte (35.7 cP at 25 °C). However, the formation of nanotubes with a close-packed architecture in our study indicates that, because of the low viscosity of the EG electrolyte (16.9 cP at 25 °C), the capillary force on the nanotube surface is not strong enough to bend the nanotubes during the growth, thus resulting in closely packed nanotubes. The growth mechanism of such closely packed nanotubes and formation of ripples are discussed further in detail.

dx.doi.org/10.1021/am402203m | ACS Appl. Mater. Interfaces 2013, 5, 9026−9033

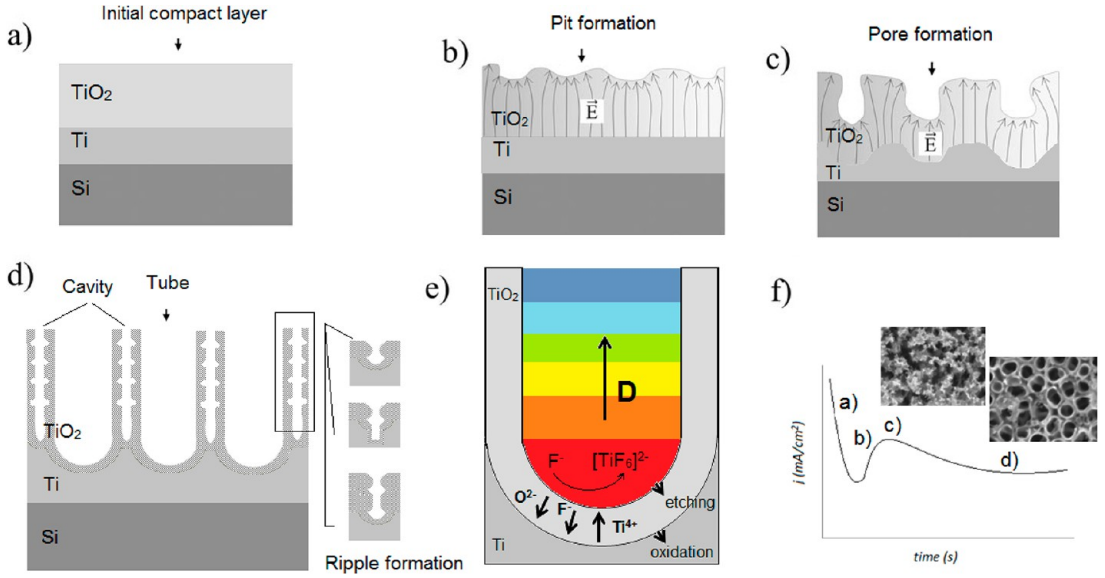

Figure 3. Schematic representation of the growth mechanism of TFTN arrays on silicon in electrochemical anodization: (a) formation of the compact anodic oxide; (b) local field distribution correlated to the surface morphological fluctuations; (c) initiation of the pore growth due to the field-enhanced dissolution; (d) pore growth to form tubes in steady-state conditions; (e) overall growth mechanism including oxidation and etching steps; (f) current−time curve monitored during the electrochemical growth in an aqueous solution and corresponding effect on the morphology of the film shown in FESEM images. Images a−d were reprinted with permission from Ghicov et al.[23] Copyright 2009 The Royal Society of Chemistry.

Figure 3 shows a schematic representation of the TFTN array under anodic conditions. The formation of nanotubes in electrochemical anodization is a self-ordering process in which the degree of ordering is dependent on the electrolyte (pH), voltage, temperature, and presence of impurities in the material.[23] The mechanism of tube formation is shown in Figure 3, which is explained in detail in the following. The first step of growth is controlled by the applied field and begins with TiO_2 formation [by oxidation of the titanium layer, as shown in Figure 3a and based on eq 2, and continuing with solvatization of Ti^{4+} (eq 3)]. The applied field acts as the driving force for ionic transport through the barrier layer at the bottom of the pore. Under the applied field, the Ti^{4+} ions migrate outward, while O^{2-} ions migrate toward the metal−oxide interface (Figure 3b). Yasuda et al. have found that nanopore/nanotube diameters correlate linearly with the growth factor of the transition-metal oxide [the growth factor $f_{growth} = t_{film}/\Delta U$ in which t_{film} is the (compact) oxide thickness that grows at a specific voltage in a metal and ΔU is the potential difference through the film].[24] In fact, because of local changes in the thickness of the oxide layer over the surface, the distribution of the electric field is varied, which results in anisotropy in the field-assisted oxidation/etching process. As the process proceeds, the pores start to form locally through dissolution of the oxide at specific sites on the surface due to F^- ion attack directed by the local field distribution correlated to the surface morphological fluctuations, as shown in Figure 3c. From these point sources, the oxide growth would take place immediately in all directions, resulting in a hemispherical oxide structure with a certain radius $R = f_{growth}U$. Repeated breakdown at the bottom of the pores would then lead to an oxide tube diameter proportional to the oxidation factor of the metal.[25] As the chemical dissolution proceeds in the barrier layer, the electric field in these thinned regions increases, enhancing the field-assisted oxide growth and oxide dissolution. Thus, well-defined interpore cavities start forming as if the entire growth process has started over in these regions, as shown in Figure 3d. At this point, depending on the amount of water in the electrolyte, the ripples start to appear as a result of such a repeating field-assisted oxidation/thinning/dissolution process. Thereafter, both cavities and tubes grow in parallel and form the tube walls. The nanotube length increases until the electrochemical etch rate equals the chemical dissolution rate of the top surface of the nanotubes. Such chemical dissolution is the key step for formation of the nanotube arrays. At this step, the thinning process of the barrier layer is continued to keep the electrochemical etching (field-assisted oxidation and dissolution) process active. No nanotubes can be formed if chemical dissolution is too high or too low.[5]

In later growth stages, reactions continue in a steady-state condition under competition between the tube growth at the bottom and chemical/electrochemical dissolution (eqs 4 and 5) at the top.[23] In the case of an aqueous electrolyte, it was found that these two competing processes are dependent on the anodization temperature. At this point, the process becomes diffusion-controlled and thereby the growth can become affected by the viscosity of the electrolyte. At temperatures higher than 5 °C, the surface of the nanotubes was found to be covered with some irregular features indicating a higher dissolution rate of the oxide. At a low-temperature range of 2−5 °C, precipitate-free nanotubes were found to be formed at a sufficiently low rate of the chemical dissolution of TiO_2. A constant field gradient is established in the bottom of the tube that determines ion transport, resulting in the development of a diffusion profile (D) within the tube, as shown in Figure 3e. By monitoring the current changes during the anodization process, one can control the growth process to optimized conditions. The growth mechanism can be summarized in four steps as follows:

Field-assisted oxidation:

$$Ti + 2H_2O \rightarrow TiO_2 + 4H^+ + 4e^- \quad (2)$$

dx.doi.org/10.1021/am402203m | ACS Appl. Mater. Interfaces 2013, 5, 9026−9033

Field-assisted migration:

$$Ti^{4+} + 6F^{-} \rightarrow [TiF_6]^{2-} \quad (3)$$

Field-assisted dissolution:

$$TiO_2 + 6F^{-} + 4H^{+} \rightarrow [TiF_6]^{2-} + 2H_2O \quad (4)$$

Chemical dissolution:

$$TiO_2 + 6HF \rightarrow [TiF_6]^{2-} + 2H_2O + 2H^{+} \quad (5)$$

Figure 4a shows the TEM image of the crystalline TFTNs formed in an aqueous electrolyte with ripples formed on the entire length of the tubes. However, in the case of organic TFTNs (Figure 4b), the sidewalls are formed as straight and smooth lines with no gap between them. This effect is attributed to the presence of water as a higher fluoride-containing medium between the nanotubes increases the chemical dissolution rate of the oxide, thus causing faster local etching of the nanotubes, as explained earlier. The diffraction patterns shown in the insets reveal the polycrystalline nature of the nanotubes with the (101), (004), (200), and (105) planes corresponding to the tetragonal titania anatase in both samples. In the case of aqueous TFTNs, the diffuse diffraction spots in the pattern indicate the presence of lattice disorder and defects in the structure. However, in the case of organic TFTNs, the presence of distinct diffraction spots confirms the presence of perfect crystals.

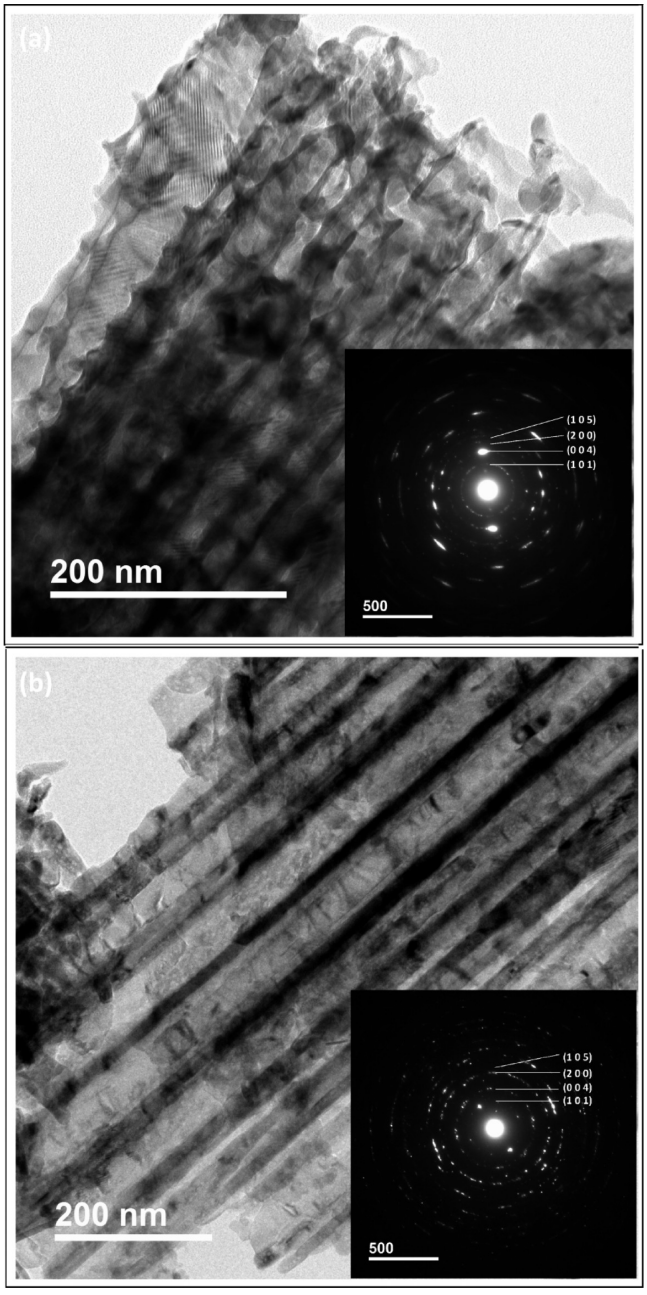

Figure 4. TEM images of (a) aqueous and (b) organic TFTN arrays and the corresponding diffraction patterns (insets).

In order to study crystallization during thermal annealing of the as-anodized TFTNs, in situ HT-GIXRD was used to detect the information about the crystalline phases only from the film. The as-anodized organic TFTN sample was heated from room temperature to 450 °C at a heating rate of 1 °C/min in air, and the XRD patterns were recorded using a glancing angle of 1° at different temperature increments from room temperature up to 450 °C. The sample was then annealed at 450 °C for 4 h followed by recording of the XRD patterns after annealing at 450 °C and cooling to room temperature, at 25 °C. As shown in Figure 5a, the film starts to form the crystalline anatase TiO_2 at 350 °C with the main characteristic peak of the (101) plane at a diffraction angle of 25° and those of the (004), (200), and (105) planes shown at 36°, 48°, and 54° (ICDD PDF 01-071-1176), respectively. XRD analysis on both aqueous and organic samples revealed that the onset of the crystallization temperature in TFTN is slightly lower than that of the TiO_2 nanotubes grown on a titanium film.[11]

Parts a and b of Figure 5 show high-resolution XPS spectra of Ti 2p and O 1s of the organic TFTN array sample after heat treatment. Ti 2p has two peaks corresponding to Ti $2p_{3/2}$ and Ti $2p_{1/2}$ photoemission spectra observed at 459.5 and 465.2 eV, respectively, with a spin−orbit splitting of 5.7 eV, indicating (as expected) the Ti^{4+} chemical state. Figure 5c shows O 1s photoemission spectra at 531 eV, which corresponds to the oxygen bonded to Ti^{4+}. The shoulder peak on the higher-binding energy side of the main O 1s peak at approximately 532.5 eV originates from adsorption of the hydroxyl groups on the surface. The Ti 2p and O 1s peak positions were found to be in agreement with the Ti−O binding energies in TiO_2 after annealing, confirming the formation of titanium oxide.

3.2. TFTN Growth on FIB Micropatterned 3D Isolated Islands. In order to investigate the mechanism of TiO_2 nanotube growth on 3D isolated islands, the sputtered titanium film was patterned using a FIB before anodization. This approach has enabled us to use the accuracy of the FIB technique in the creation of smooth surfaces in isolated islands to investigate the growth mechanism of the nanotubes on such surfaces, a specific novel feature that has not been achieved in photolithography-based techniques, as reported previously by Chappanda et al.[15] The patterned thin film was then anodized under the same conditions as those used for the synthesis of the organic TFTN sample. Figure 6 shows FESEM images of the as-anodized and annealed FIB micropatterned cylindrical and cubic arrays of isolated 3D islands, each with a volume of ~78.5 and ~100 μm^3, respectively, on the titanium film. The thickness of the titanium film is ~1.6 μm, which can be distinguished from the silicon substrate based on the contrast in the SEM image. The presence of small cracks on the surface is due to the local heat generated from the high energy of the FIB.

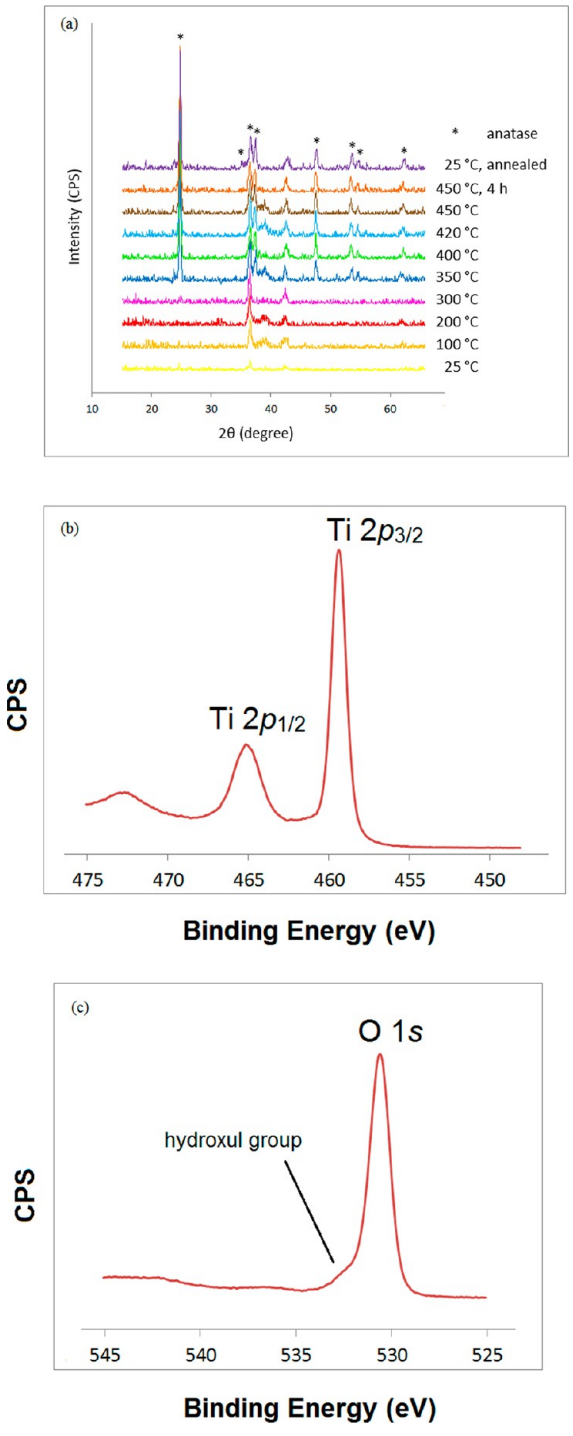

Figure 5. (a) HT-GAXRD patterns of TFTN as a function of the annealing temperature. (b and c) High-resolution XPS spectra of the Ti 2p and O 1s peaks of an annealed organic TFTN array sample.

Formation of the TiO_2 nanotube array is influenced by three main factors. In 3D isolated islands, the titanium layer is in electrical contact with a conductive substrate (silicon) only along the base and not at the sidewalls; thus, the growth is only guided by the charge path combined with distribution of the electrical field in the titanium layer underneath. The EDS elemental map and chemical composition of the TiO_2 islands after anodization are shown in Figure S1 (in the Supporting Information). According to this map, the presence of titanium and oxygen only on the patterned areas versus the silicon in the milled area confirms that the patterned regions are electrically isolated from the titanium layer and its surroundings. As seen in Figure 6e,f, uniform growth of the nanotubes can be observed on both types of geometries, particularly, at the edges and sidewalls of the islands. Moreover, the porous surface of the nanotube arrays is extended from the top to the sidewalls of the islands without any trace of nanotube walls at the edges.

In order to understand the mechanism of growth of nanotubes at the sidewalls of the islands, a close-view FESEM micrograph of typical annealed TFTN arrays on the cylindrical island is taken by making a cut section in the middle of the island and at the edge. As seen in Figure 7a, the cut-section area in the middle of the island (red line in Figure 7b) reveals the formation of vertically oriented nanotubes, as expected. Clearly, because of the excess of O^{2-} and F^- ions in the electrolyte adjacent to the surfaces of the 3D islands at the top and sidewalls, growth of TiO_2 nanotubes involves initially formation of the porous structure via fast diffusion of O^{2-} from the surfaces and oxidation of Ti to Ti^{4+}; this step competes later with dissolution of TiO_2 by incorporation of the F^- ions in the growing TiO_2 lattice, which forms the water-soluble TiF_6^{2-} complexes; meanwhile, the growth is controlled by distribution of the electrical field gradually from the vertical to horizontal direction. As the surface starts to curve on the edges, the nanotubes tend to gradually orient according to the surface curvature, while they are still interconnected at the roots. In fact, this orientation results from deflection of the nanotubes on the walls of islands guided by the change in the direction of the electric field normal to the surface plane and outward to the surface in such a way that the open side of the nanotubes is always in the direction of the surface normal, while its closed end is connected to the TiO_2 barrier layer (Figure 7c). While ion diffusion is uniformly possible from each side of the island walls, the larger electrical field at the edges of the curved sidewalls of the islands results in concentration of the F^- ions at the edges between the sidewalls of the islands and their surface; thus, TiF_6^{2-} dissolution competes the TiO_2 formation and results in the formation of a strip of nanoporous structures at the edges. The schematic of Figure 7d demonstrates the mechanism of growth of deflected nanotubes under an applied electric field as we get close to the sidewalls of the islands.

4. CONCLUSION

The electrochemical growth of self-organized TFTN arrays on a silicon substrate via anodization of sputtered titanium on silicon is shown through two different routes. Vertically oriented nanotube arrays with an average diameter of ~30 nm and a length of ~1.5 μm are synthesized at different potentials and growth times in aqueous and organic-based types of electrolytes. It was shown that the low-temperature growth of TFTNs in an aqueous HF-based electrolyte leads to the complexity of the process, and the nanotubes show lower quality compared to the organic-based NH_4F electrolyte. The fabrication and growth mechanism of TFTN arrays on 3D isolated islands were successfully demonstrated using a one-step FIB technique. It was shown that the growth of TFTN on 3D isolated areas is affected by the distribution of the electric field in the 3D region as well as field-enabled transport of mobile ions, resulting in the formation of deflected nanotubes on the sidewalls of the islands. This work demonstrates the use of the FIB technique as a simple, high-resolution, and maskless method for high-aspect-ratio etching for the creation of isolated islands and shows great promise toward the use of the

dx.doi.org/10.1021/am402203m | ACS Appl. Mater. Interfaces 2013, 5, 9026−9033

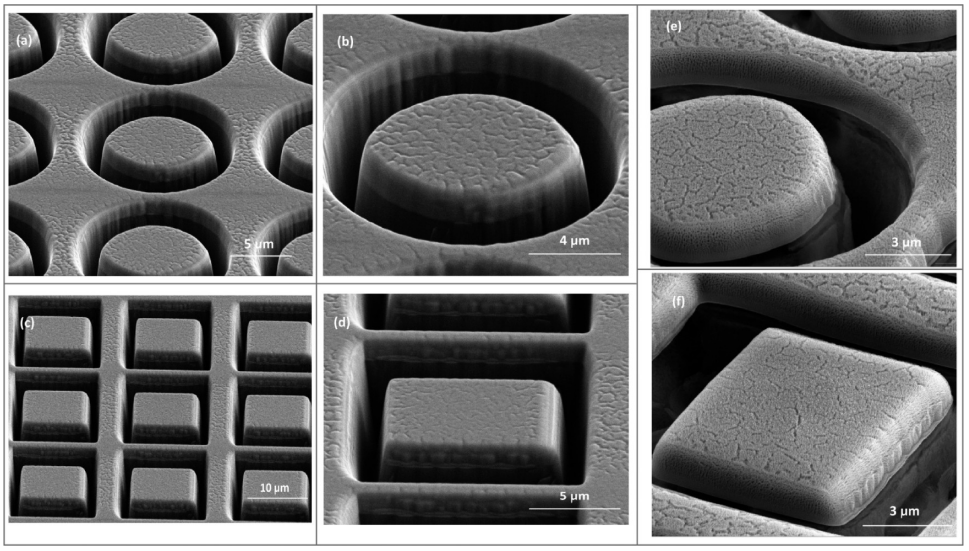

Figure 6. Cross-sectional view of FESEM images of the FIB: (a–d) as-anodized and (e and f) annealed micropatterned cylindrical and cubic arrays of 3D isolated islands on a titanium film in different magnifications.

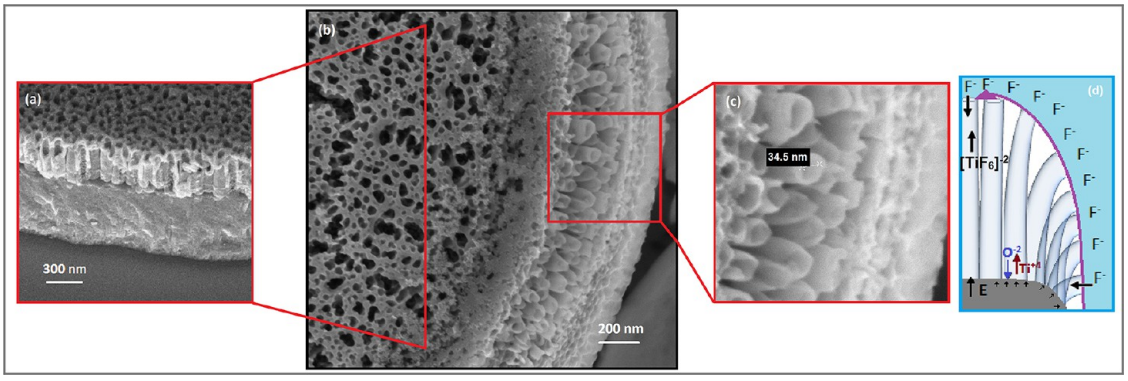

Figure 7. (a) Cross-sectional view of the FESEM micrograph of the marked line in part b, which shows the top view of the FESEM micrograph of the TiO_2 nanotube arrays in a cylindrical island after annealing. (c) High-magnification FESEM micrograph of the marked area on part b showing gradually deflecting nanotubes grown on the sidewall of the island. (d) Schematic showing the mechanism of growth of deflected nanotubes under an applied electric field.

proposed approach for the development of metal–oxide nanostructured devices and their integration with micro- and nanoelectromechanical systems and integrated-circuit devices.

■ ASSOCIATED CONTENT

Ⓢ Supporting Information

FESEM images of the as-anodized TFTNs grown on FIB micropatterned 3D islands and the EDS elemental map of a typical cylindrical island showing chemical composition of the TiO_2 islands after anodization, which confirms electrical isolation of the patterned region and the titanium surroundings. This material is available free of charge via the Internet at http://pubs.acs.org.

■ AUTHOR INFORMATION

Corresponding Author

*E-mail: hamani3@gatech.edu.

Notes

The authors declare no competing financial interest.

■ ACKNOWLEDGMENTS

This work was funded by Pacific Northwest National Laboratory. The TEM work was carried out at Florida State University (FSU), and the TEM facility at FSU is funded and supported by the Florida State University Research Foundation, National High Magnetic Field Laboratory (Grant NSF-DMR-0654118), and the State of Florida. The authors would like to thank Eric Woods from Georgia Institute of Technology's Institute for Electronics and Nanotechnology (IEN) for the FIB micropatterning advice.

■ REFERENCES

(1) Kuypers, J. H.; Zolfagharkhani, G.; Gaidarzhy, A.; Thalmayr, F.; Sparks, A.; Chen, D. M.; Rebel, R.; Newman, B.; Asmani, M.; Badillo, D.; Schoepf, K. J. *Proc. IEEE Int. Freq. Control Symp.* **2012**, 1–5.

(2) Robinson, J. T.; Jorgolli, M.; Shalek, A. K.; Yoon, M.-H.; Gertner, R. S.; Park, H. *Nat. Nanotechnol.* **2012**, *7*, 180–184.

(3) Kuan-Lun, C.; Gold, S.; Subramanian, V.; Chang, L.; Shannon, M. A.; Masel, R. I. *J. Microelectromech. Syst.* **2006**, *15*, 671–677.

(4) Lu, H. F.; Li, F.; Liu, G.; Chen, Z.-G.; Wang, D.-W.; Fang, H.-T.; Lu, G. Q.; Jiang, Z. H.; Cheng, H.-M. *Nanotechnology* **2008**, *19*, 405504–405511.

(5) Shankar, K.; Basham, J. I.; Allam, N. K.; Varghese, O. K.; Mor, G. K.; Feng, X.; Paulose, M.; Seabold, J. A.; Choi, K.-S.; Grimes, C. A. *J. Phys. Chem. C* **2009**, *113*, 6327−6359.
(6) Su, X.; Wu, Q.; Zhan, X.; Wu, J.; Wei, S.; Guo, Z. *J. Mater. Sci.* **2012**, *47*, 2519−2534.
(7) Rettew, R. E.; Allam, N. K.; Alamgir, F. M. *ACS Appl. Mater. Interfaces* **2011**, *3*, 147−151.
(8) Ortiz, G. F.; Hanzu, I.; Knauth, P.; Lavela, P.; Tirado, J. L.; Djenizian, T. *Electrochim. Acta* **2009**, *54*, 4262−4268.
(9) Varghese, O. K.; Paulose, M.; Grimes, C. A. *Nat. Nanotechnol.* **2009**, *4*, 592−597.
(10) Macak, J. M.; Tsuchiya, H.; Berger, S.; Bauer, S.; Fujimoto, S.; Schmuki, P. *Chem. Phys. Lett.* **2006**, *428*, 421−425.
(11) Mor, G. K.; Varghese, O. K.; Paulose, M.; Shankar, K.; Grimes, C. A. *Sol. Energy Mater. Sol. Cells* **2006**, *90*, 2011−2075.
(12) Roy, P.; Berger, S.; Schmuki, P. *Angew. Chem., Int. Ed.* **2011**, *50*, 2904−2939.
(13) Hamedani, H. A.; Allam, N. K.; Garmestani, H.; El-Sayed, M. A. *J. Phys. Chem. C* **2011**, *115*, 13480−13486.
(14) Allam, N. K.; Alamgir, F.; El-Sayed, M. A. *ACS Nano* **2010**, *4*, 5819−5826.
(15) Chappanda, K. N.; Smith, Y. R.; Misra, M.; Mohanty, S. K. *Nanotechnology* **2012**, *23*, 38601−38609.
(16) Masuda, Y.; Ieda, S.; Koumoto, K. *Langmuir* **2003**, *19*, 4415−4419.
(17) Lai, Y.; Huang, J.; Gong, J.; Huang, Y.; Wang, C.; Chen, Z.; Lin, C. *J. Electrochem. Soc.* **2009**, *156*, D480−D484.
(18) Pittrof, A.; Bauer, S.; Schmuki, P. *Acta Biomater.* **2011**, *7*, 424−431.
(19) Chen, B.; Lu, K. *Phys. Chem. Chem. Phys.* **2012**, *15*, 1854−1862.
(20) Chen, B.; Lu, K.; Tian, Z. *J. Mater. Chem.* **2011**, *21*, 8835−8840.
(21) Berger, S.; Hahn, R.; Roy, P.; Schmuki, P. *Phys. Status Solidi B* **2010**, *247*, 2424−2435.
(22) Mohammadpour, A.; Waghmare, P. R.; Mitra, S. K.; Shankar, K. *ACS Nano* **2010**, *4*, 7421−7430.
(23) Ghicov, A.; Schmuki, P. *Chem. Commun.* **2009**, *0*, 2791−2808.
(24) Yasuda, K.; Ghicov, A.; Nohiraa, T.; Kani, N.; Hagiwara, R.; Schmuki, P. *Electrochem. Solid-State Lett.* **2008**, *11*, C51−C54.
(25) Macak, J. M.; Tsuchiya, H.; Ghicov, A.; Yasuda, K.; Hahn, R.; Bauer, S.; Schmuki, P. *Curr. Opin. Solid State Mater. Sci.* **2007**, *11*, 3−18.